 MCB, vol.8, no.1, pp.1-20, 2011

Influence of Arterial Wall Compliance on the Pressure Drop across Coronary Artery Stenoses under Hyperemic Flow Condition

Bhaskar Chandra Konala[*], **Ashish Das**[*] **and Rupak K Banerjee**[*,†]

Abstract: Hemodynamic endpoints such as flow and pressure drop are often measured during angioplasty procedures to determine the functional severity of a coronary artery stenosis. There is a lack of knowledge regarding the influence of compliance of the arterial wall-stenosis on the pressure drop under hyperemic flows across coronary lesions. This study evaluates the influence in flow and pressure drop caused by variation in arterial-stenosis compliance for a wide range of stenosis severities.

The flow and pressure drop were evaluated for three different severities of stenosis and tested for limiting scenarios of compliant models. The Mooney-Rivlin model defined the non-linear material properties of the arterial wall and the plaque regions. The non-Newtonian Carreau model was used to model the blood flow viscosity. The fluid (blood)-structure (arterial wall) interaction equations were solved numerically using the finite element method.

Irrespective of the stenosis severity, the compliant models produced a lower pressure drop than the rigid artery due to compliance of the plaque region. A wide variation in the pressure drop was observed between different compliant models for significant (90% area occlusion) stenosis with 41.0, 32.1, and 29.8 mmHg for the rigid artery, compliant artery with calcified plaque, and compliant artery with smooth muscle cell proliferation, respectively. When compared with the rigid artery for significant stenosis the pressure drop decreased by 27.7% and 37.6% for the calcified plaque and for the smooth muscle cell proliferation case, respectively. These significant variations in pressure drop for the higher stenosis may lead to misinterpretation and misdiagnosis of the stenosis severity.

Keywords: Coronary artery stenosis, Fluid-structure interaction, Arterial wall

[*] Department of Mechanical Engineering, University of Cincinnati, Cincinnati, OH

[†] Department of Mechanical Engineering, 593 Rhodes Hall, ML 0072, University of Cincinnati, Cincinnati, Ohio, 45221. Phone: 513-556-2124; Fax: 513-556-3390; Email: Rupak.Banerjee@uc.edu

compliance, pressure drop, blood flow, hemodynamics

Nomenclature

t	time in sec
r	radius in cm
d	diameter in cm
p	pressure in mmHg
u	velocity in cm/sec
σ	stress in dynes/cm^2
T	period of cardiac cycle
Q	blood flow rate
ρ	blood density

Superscripts

$\sim$	time averaged
S	solid (arterial wall and plaque region)
D	fluid (blood flow)
$\cdot$	time derivative

Subscripts

z	axial
r	radial
c	circumferential
i, j	coordinate directions
a	proximal to the stenosis
o	distal to the stenosis

1 Introduction

Coronary artery disease (CAD) was the cause for one of every six deaths in the United States in 2006 (1). Plaque formation in the *left anterior descending* (LAD) is one of the major causes of angina and heart failure. Geometric or anatomical measurements using techniques like contrast angiography, angioscopy and intravascular ultrasound are frequently used to assess the ischemic severity of epicardial

coronary stenosis. However, they are difficult to measure due to the hemodynamic implications and thus may not generate accurate information regarding the severity of coronary stenosis (2). Functional or hemodynamic measurements of overall pressure drop/gradient across the stenosis and flow rate were proved to be more useful for the long term success of coronary intervention such as balloon angioplasty (3) with or without stent placement procedure.

An improved understanding of the stenotic flows could be obtained from *in vitro* measurements by Young and Tsai (4), Mates et al. (5), Cho et al. (6) and computational studies by Deshpande et al. (7) and Siegel et al. (8), for steady laminar flows through vascular stenoses, and by Back et al. (9) for pulsatile flow in a stenosed coronary artery casting. The importance of image-based computational fluid dynamics (CFD) in monitoring hemodynamics and atherosclerosis was discussed by Steinman et al. (10). The hemodynamic parameters for flow through coronary stenoses for varying severities were studied earlier by our research group using in-vivo and in-vitro measurements and CFD (11-24). Bathe et al. (25) have studied the fluid (blood)-structure (arterial wall) interaction (FSI) using finite element analysis for pulsatile blood flow through a compliant stenotic artery. Tang et al. have also performed FSI computations for various coronary artery stenosis models to study plaque vulnerability (26) and stress-strain distributions along the arterial wall (27). Valencia et al. (28, 29) have studied the hemodynamic parameters such as wall shear stress and pressure drop with respect to inlet velocity in compliant stenotic cerebral arteries.

However, none of the studies have reported the influence of arterial wall-stenosis compliance on hemodynamic endpoints under variable stenotic severities at hyperemic flows. This study is unique as we have reported the influence of compliance on the pressure drop across coronary artery stenoses for different levels of stenosis severity. Fluid-structure interaction (FSI) analysis was used to simulate the arterial wall-stenosis compliance and blood flow interactions using numerical calculations. These calculations can eventually assist in better functional (hemodynamic) diagnosis of coronary artery stenosis under clinical setting.

2 Methods

The stenosis geometry for the present study was considered to be a single-vessel, single-lesion epicardial coronary artery disease (30). Three different severities of coronary artery stenoses, 70% (moderate), 80% (intermediate) and 90% (severe) area blockages, were modeled to evaluate the effect of coronary arterial wall-stenosis compliance on the pressure drop (Δp) under hyperemic flows. The following models were used to assess the effect of compliance: *rigid artery* (RA; baseline case representing high wall elasticity), *compliant artery with calcified plaque* (CP;

representing intermediate wall elasticity) and *compliant artery with smooth muscle cell proliferation* (SP; representing lower wall elasticity). In addition to the above three cases of stenosis severity, a 64% stenosis case was also evaluated using only RA wall model for comparison with previously reported clinical (pre-angioplasty and post-angioplasty) data (30).

2.1 Blood Flow (Fluid) Model

The coronary artery geometry used for this study was based on the dimensions of a focal lesion (Table 1) reported by Wilson et al. for a 32-patient group undergoing percutaneous transluminal balloon coronary angioplasty (PTCA) (14, 30). The geometries were adapted from biplanar X-ray angiography images obtained by the Wilson et al. (1998) study mentioned above. The additional dimensional data on the lesion shape were used from a similar stenosis described by Back and Denton (31) and Roy et al. (17). The dimensional data for the three stenosis severities have been provided in Table 1.

Table 1: Dimensional data for the four stenosis severities, 64%, 70%, 80%, and 90% area stenosis. r_e= Radius of native artery, l_c = Length of converging region, r_m = Radius of throat region,l_m = Length of throat region, l_r = Length of diverging section, t_e = Thickness of arterial wall, t_m = Thickness of physiologic material over plaque.

% Area Stenosis	All dimensions in mm						
	r_e	t_e	r_m	l_c	l_m	l_r	t_m
64	1.5	1	0.90	6	3.0	1.5	0.1
70	1.5	1	0.82	6	3.0	1.5	0.1
80	1.5	1	0.67	6	1.5	1.5	0.1
90	1.5	1	0.47	6	0.75	1.5	0.1

The blood flow through the stenosed coronary arteries was considered to be unsteady (pulsatile) and incompressible. Blood was modeled to be a non-Newtonian viscous fluid. The governing equations were the continuity and momentum equations with the Arbitrary Lagrangian Eulerian (ALE) formulation,

$$\nabla.u = 0 \quad \text{(continuity equation)} \tag{1}$$

$$\rho(\partial u/\partial t + ((u-u_m).\nabla)u = -\nabla p + \nabla.(\mu\nabla u) \text{ (momentum eq.)} \tag{2}$$

where u_m is the mesh velocity in cm/sec, μ is the dynamic viscosity in Poise and ρ is the density in gm/cm^3. The non-Newtonian Carreau model was used to model the shear rate ($\dot{\gamma}$; 1/sec)dependent blood viscosity (32).

$$\mu = \mu_\infty + (\mu_0 - \mu_\infty).(1 + (\beta\dot{\gamma})^2)^{(n-1)/2} \tag{3}$$

where the coefficients are given as: the zero shear rate viscosity, μ_0= 0.56 Poise, infinite shear rate viscosity, μ_∞= 0.0345 Poise, time constant, β = 3.313 sec, and power index, n = 0.3568. The density (ρ) of blood was taken as 1.05 gm/cm^3.

The following boundary conditions have been applied:

$$\text{Pressure at inlet } = p_a(t) \tag{4}$$

$$\text{Flow at the outlet } = Q_0(t) \tag{5}$$

$$\partial u/\partial z = 0 \quad \text{at the inlet and outlet} \tag{6}$$

$$\text{Radial velocity, } u_r, \text{ at the axis } = 0 \tag{7}$$

A no slip boundary condition was applied at the vessel lumen and arterial wall interface.

$$u = \dot{d}^s \tag{8}$$

where $\dot{d}$ is the time derivative of displacement in cm at the fluid and solid interface.

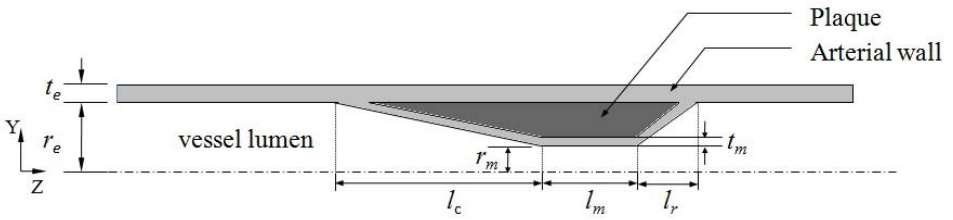

Figure 1: Geometric model of the stenosed coronary artery

A physiological pressure profile for a human coronary artery, $p_a(t)$, [Fig. 2A] obtained from Tang et al. (26) was applied at the inlet. A coronary flow waveform, $Q_0(t)$, [Fig. 2B] which was obtained from in-vitro calibration and by smoothing the Doppler fluctuating effect, with a parabolic velocity profile, was specified at the outlet (6). The spatial velocity profile was considered to be of parabolic shape at all time instants. Since the downstream vessel was extended by 7 cm (more than

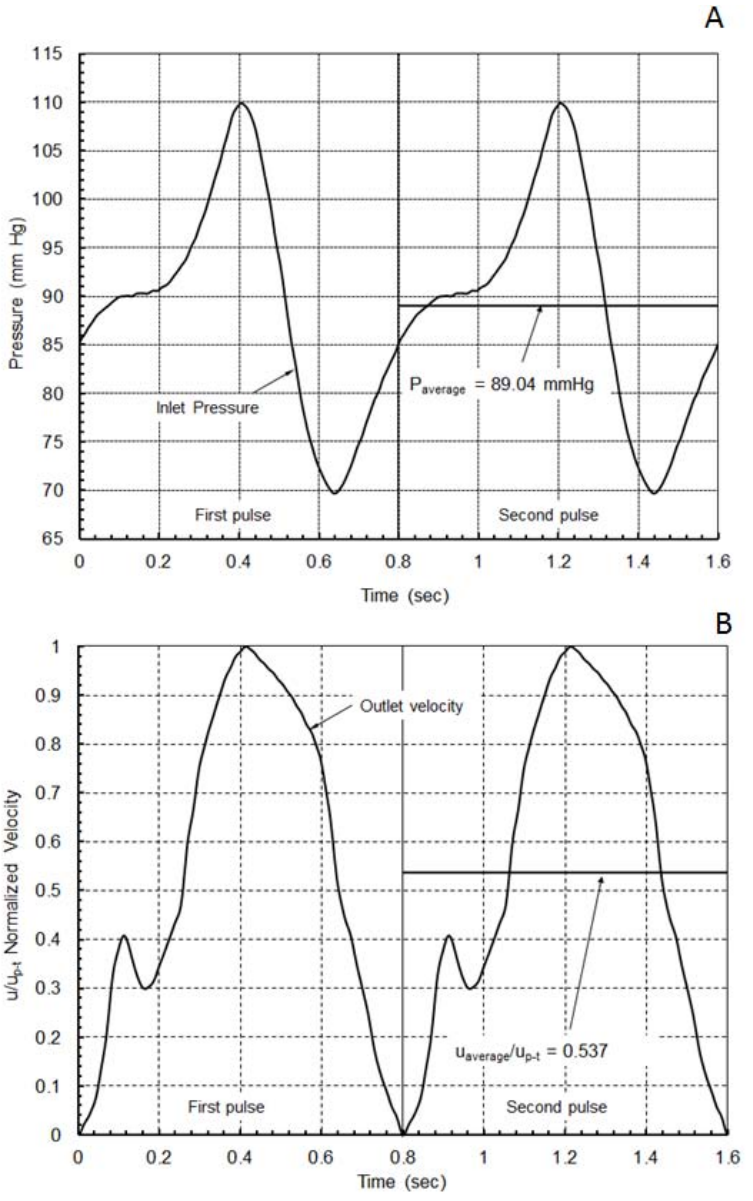

Figure 2: (A) Time varying inlet pressure and (B) Normalized velocity pulse specified at the outlet

20 times of the vessel diameter) distal to the stenosis the influence of the spatial outlet boundary condition on the flow field near the stenosis region was negligible (13-16). The normal flow pattern was shifted for the distal left anterior descending artery. The pattern was phase shifted to maintain a 4^o phase difference between the pressure and flow. The peak velocity u_{p-t} shown in Fig. 2B was normalized to 1.0, so that the ratio of mean to peak velocity u/u_{p-t} is 0.537. The hyperemic mean flow rates (30) of 175 ml/min, 165 ml/min and 115 ml/min were used for the moderate (70%), intermediate (80%), and severe (90%) area stenoses, respectively. For the 64% area stenosis case, a hyperemic mean flow rate of 180 ml/min was used to perform the rigid wall-blood flow computations. These values were obtained from multiplying a typical basal physiological flow rate value of $\tilde{Q}$= 50 ml/min for a 3 mm coronary vessel (9) with the Coronary Flow Reserve (CFR) values from Roy et al. (17, 30).

2.2 Arterial Wall-Stenosis (Solid) Model

The thickness of the LAD arterial wall was considered as 1 mm (33). A physiological skin over the plaque region was modeled with a thickness of 0.1 mm and with similar material properties as the arterial wall. Using these assumptions, dimensions for the geometric model of the arterial wall and stenosis were designed based on previously reported fluid model (13-16). The dimensions are provided in Table 1.

The arterial wall material and the plaque were assumed to be incompressible, homogeneous and hyperelastic. The boundary conditions and equilibrium states are discussed below:

$$\sigma^S_{ij,j} = 0 \tag{9}$$

$$\sigma^S_{ij}.n_j = \sigma^F_{ij}.n_j \text{ at the lumen-wall interface} \tag{10}$$

$$d^S = d^F \quad \text{at the inner wall} \tag{11}$$

$$\sigma^S_{ij}.n_j = 0 \quad \text{at the outer wall} \tag{12}$$

where σ^S_{ij}, σ^F_{ij} are the stress tensors in dynes/cm^2 and d^S, d^F are the displacements in cm for the arterial wall and blood flow models respectively. n is the unit vector normal to the boundary.

A modified Mooney-Rivlin (M-R) model was used to define the non-linear material properties of the arterial wall and the plaque regions (26, 34). A *transversely* isotropic strain energy density function was used which includes an additional orthotropic term to the modified M-R model.

$$W = W_{isotropic} + W_{orthotropic} \tag{13}$$

where

$$W_{isotropic} = C_1(I_1 - 3) + D_1[\exp(D_2(I_1 - 3)) - 1] \tag{14}$$

$$W_{orthotropic} = (K_1/2K_2)[\exp[K_2(I_4 - 1)^2] - 1] \tag{15}$$

I_1 is the first invariant.

$$I_4 = C_{ij}(n_c)_i(n_c)_j \tag{16}$$

C_{ij} is the Cauchy Green deformation tensor
n_c is the circumferential direction of the vessel

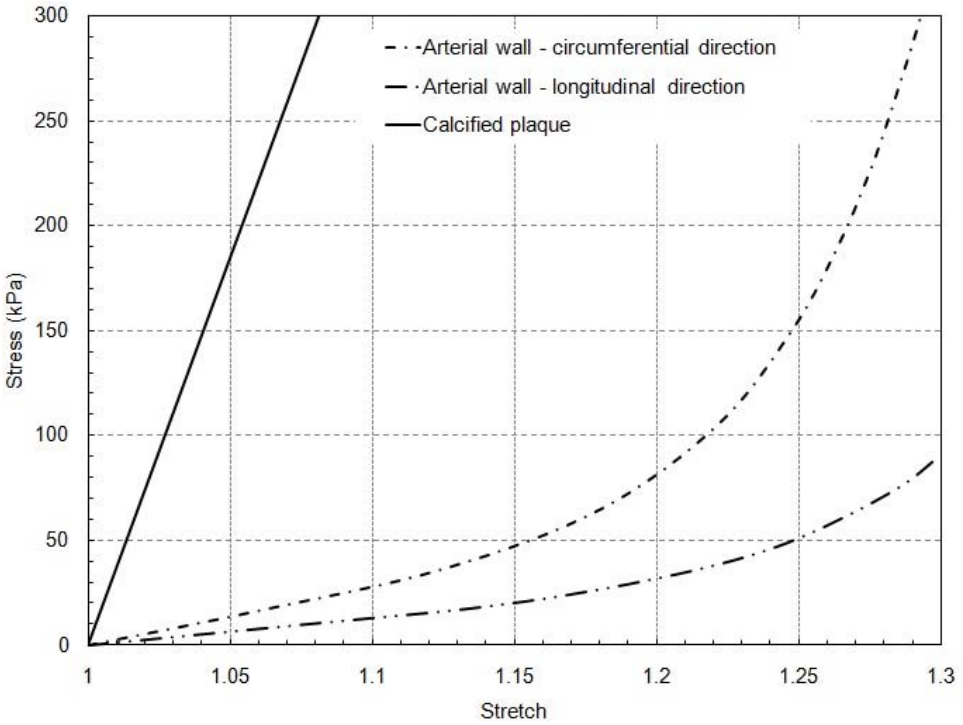

Figure 3: Mooney Rivlin model fit for stress - strain data (Tang et al., 2009)

The arterial wall for all models and the plaque region for the compliant artery with smooth muscle cell proliferation (SP) were modeled using Eq. 13. This M-R model was fit for the longitudinal and circumferential stress-stretch data as shown in Fig. 3. Only the isotropic expression in Eq. 13 was used to model the calcified plaque

region as an isotropic material for the compliant artery with calcified plaque (CP). The isotropic M-R model was used to fit the stress-stretch data for calcification as shown in Fig. 3. For calcified plaque:

$$W = W_{isotropic} = C_1(I_1 - 3) + D_1[\exp(D_2(I_1 - 3)) - 1] \tag{17}$$

The values for the material constants C_1, D_1, D_2, K_1 and K_2 have been provided in Table 2 (26).

Table 2: Mooney-Rivlin constants for the material properties of the solid models

Model	Material constants (dynes/cm^2)				
	C_1	D_1	D_2	K_1	K_2
Arterial wall	82917	9072	3.1	88240	3.7
Calcified plaque	2814430	131010	11.5	--	--
Smooth muscle cell proliferation	82917	9072	3.1	88240	3.7

2.3 Computation Methodology

In order to account for the residual stresses in the artery, a two-step process of axial stretch and radial expansion was employed. Starting with a no-load radius (radius smaller than the *in vivo* radius), the artery was axially stretched by 10% of its initial length and pressurized with an average pressure of 89.04 mmHg to a stressed state such that the final dimensions were in close match with the *in vivo* dimensions (Table 1). The no-load radius (the radius of the artery before axial stretch and radial expansion) was adjusted such that the dimensions specified in Table 1 were obtained in the stressed state. Specifically, the resulting stenosis severities (obtained after axial stretch and radial expansion) for the CP case were 69.9%, 80.3%, and 89.8% and those for the SP case were 70.0%, 80.2%, and 89.6%, respectively. Thus, the resulting stenosis severity values were in close match with the idealized stenosis severities of 70%, 80% and 90% area stenosis, respectively. The time varying pressure, $p_a(t)$, and flow,$Q_0(t)$, were then applied at the inlet and outlet respectively to perform the blood flow-arterial wall interaction computations.

A structured quadrilateral mesh, with axi-symmetric elements, was used for the arterial wall (solid model) and the vessel lumen (fluid model). An unstructured triangular mesh was used for the plaque region in all models due to the sharp angles in the geometry. The finite element method was used to solve the coupled FSI

equations (ADINA R&D Inc., MA). Mesh convergence studies were performed until the solutions differed by less than 0.5%. Each computation was run for 5 cycles and it was observed that the solution does not change after the initial two cycles. The results from the last two cycles are reported here.

Compliance for a given pressure and flow pulse was calculated using the following equation:

$$\text{Compliance} = [(d_{max} - d_{min}) \times 100]/[d_{min} \times (p_{max} - p_{min})] \tag{18}$$

where p_{max} and p_{min} are the maximum and minimum pressure values in mmHg at the throat for a given pulse. d_{max} and d_{min} are the maximum and minimum diameters in cm at p_{max} and p_{min}, respectively.

3 Results

To assess the effect of compliance the models representing limiting scenarios are: *rigid artery* (RA; baseline case representing high wall elasticity), com*pliant artery with calcified plaque* (CP; representing intermediate wall elasticity) and *compliant artery with smooth muscle cell proliferation* (SP; representing lower wall elasticity). First, the compliance at the throat sections was evaluated followed by the pressure drop for different stenosis conditions.

Figure 4A, 4B and 4C shows the variation in the inner radius of the throat section over the period of one cardiac cycle for the CP and SP cases for 70%, 80%, and 90% area stenosis, respectively. It can be observed that SP showed higher variations of inner radius of throat for all the three stenosis severities. The computed mean inner radius of the throat for CP and SP case were in close agreement for all the stenosis severities (Fig. 4A, 4B, and 4C). The difference in the mean inner radius of the throat between CP and SP for 70%, 80% and 90% area stenosis were 0.04%, 0.15% (e.g. 0.15% = [{0.663-0.662}/0.662] x 100), and 0.6%, respectively. In the case of 70% area stenosis, the total radial variation, $R_{max} - R_{min}$ (where R_{max} and R_{min} are the maximum and minimum inner radii of the throat, respectively), was 0.008 mm for CP as compared to a radius variation of 0.06 mm for SP, an increase by 6.5 times. For the 80% area stenosis, the total radial variation increased by 6.8 times, from 0.009 mm for CP to 0.07 mm for SP. In the case of 90% area stenosis case, the total radius variation increased by 7.7 times, from 0.008 mm for CP to a value of 0.07 mm for SP.

Figure 5 illustrates the compliance (% diameter change / mmHg) calculated at the throat for the compliant artery with calcified plaque (CP) and the compliant artery with smooth muscle cell proliferation (SP). The compliance decreased with increase in stenosis severity in CP and increased with increase in stenosis severity

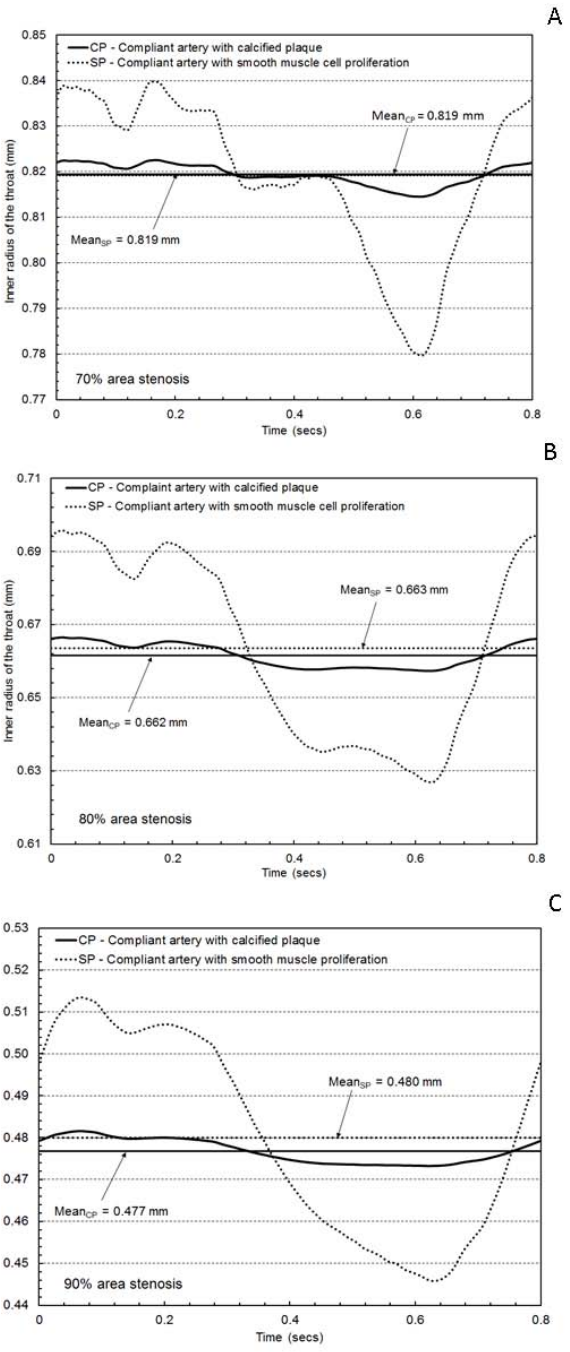

Figure 4: Variations of inner radius of the throat for compliant models at A) 70%, B) 80% and C) 90% area stenosis

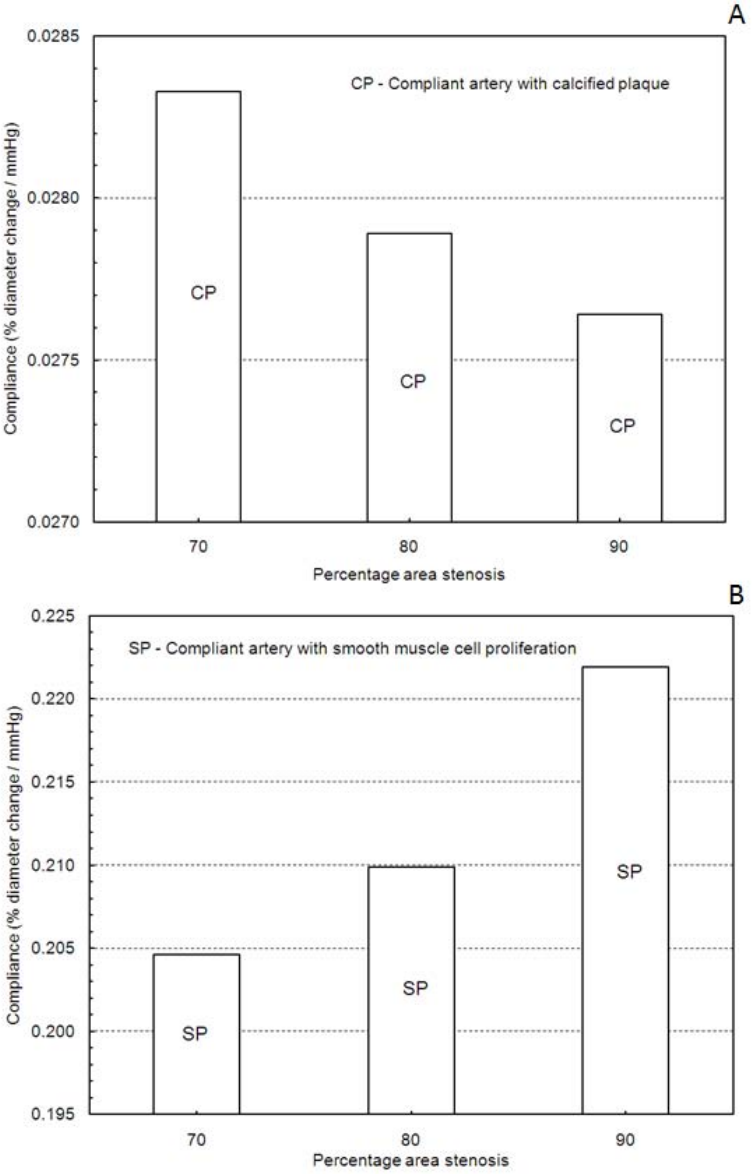

Figure 5: Compliance of the throat for (A) Compliant artery with calcified plaque and (B) Compliant artery with smooth muscle cell proliferation

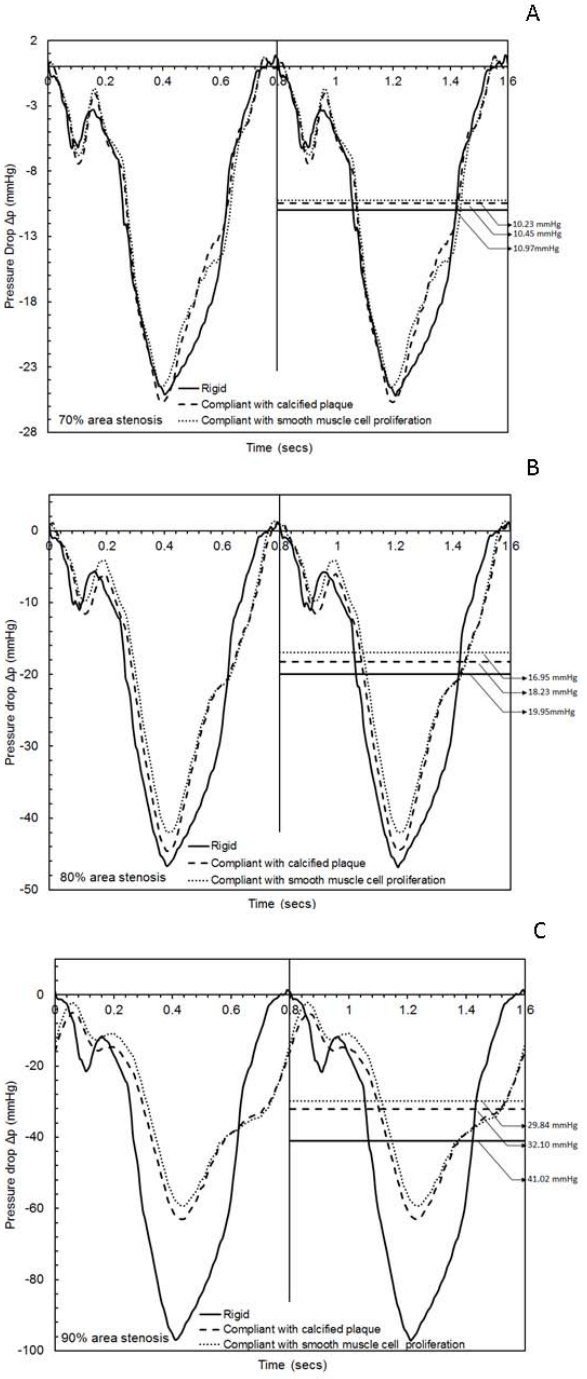

Figure 6: Time varying pressure drop for various compliant models at (A) 70% area stenosis, (B) 80% area stenosis and (C) 90% area stenosis

for SP. For CP, the compliance decreased from 0.0283% to 0.0279% per mmHg for 70% to 80% area stenosis and this value further decreased to 0.0276% per mmHg for 90% area stenosis. In the case of SP, compliance increased from 0.20% to 0.21% per mmHg for 70% to 80% area stenosis and further increased to a value of 0.22% per mmHg for 90% area stenosis. It can be seen that the CP had a lesser compliance than SP, which could be attributed to the nature of material being harder for the calcified plaque. When compared with SP, the compliance for CP decreased by 0.17%, 0.18% and 0.19% per mmHg for 70%, 80% and 90% area stenoses, respectively.

Figure 6 shows the instantaneous overall pressure drop assessed during the cardiac cycle across each of the compliant models (RA, CP, and SP) for all the three stenosis severities (70%, 80%, and 90%). Key results of all the three stenosis levels are discussed below.

70% Area Stenosis. At a mean hyperemic flow rate of 175 ml/min, the peak pressure drops were about 25.2, 25.7, and 24.5 mmHg for RA, CP, and SP, respectively. The corresponding -Δp(t) (= p_a(t) – p_o(t)), where p_a(t) and p_o(t) are the time varying pressures measured proximal and distal to the stenoses, respectively during the pulse cycle for all the cases are shown in Fig. 6A. For RA, the time averaged (mean) pressure drop value, obtained by integration over the cardiac cycle (Δp = (1/T) $\int_0^T$ Δp(t) . dt) and shown by horizontal lines in Fig. 6A, was 11.0 mm Hg. The values decreased to 10.4 mmHg by 5.7% for CP and to 10.2 mmHg by 7.8% for SP.

80% Area Stenosis. The peak pressure drops were about 46.8, 44.6, and 42.0 mmHg for RA, CP, and SP respectively, for a mean hyperemic flow rate of 165 ml/min. The corresponding -Δp(t) for all the compliant models for the pulse cycle are shown in Fig. 6B. For RA, CP, and SP, the time averaged (mean) pressure drop over the cardiac cycle (Δp), shown by horizontal lines in Fig 5B, were 19.9, 18.2 and 16.9 mmHg, respectively. When compared with RA case, the Δp decreased by 9.3% for CP and by 17.7% for SP.

90% Area Stenosis. At hyperemic mean flow rate of 115 ml/min, the peak pressure drops were about 97.1, 63.0, and 59.3 mmHg for RA, CP, and SP, respectively. The corresponding -Δp(t) for all the compliant models along the pulse cycle are shown in Fig. 6C. For RA, the time averaged (mean) pressure drop (Δp) was 41.0 mmHg (Fig 3C). When compared with RA, the Δp reduced to 32.1 mmHg, a 27.7% decrease, for CP and 29.8 mmHg, a 37.6% decrease, for SP. These are larger variations in Δp compared to the 70% and 80% area stenosis cases.

Time Averaged Pressure Drop (Δp) with Compliance. Figure 7 illustrates the Δp across the coronary stenosis for all the models considered in this study. In general the Δp increased consistently with increase in stenosis severity for all the cases. For

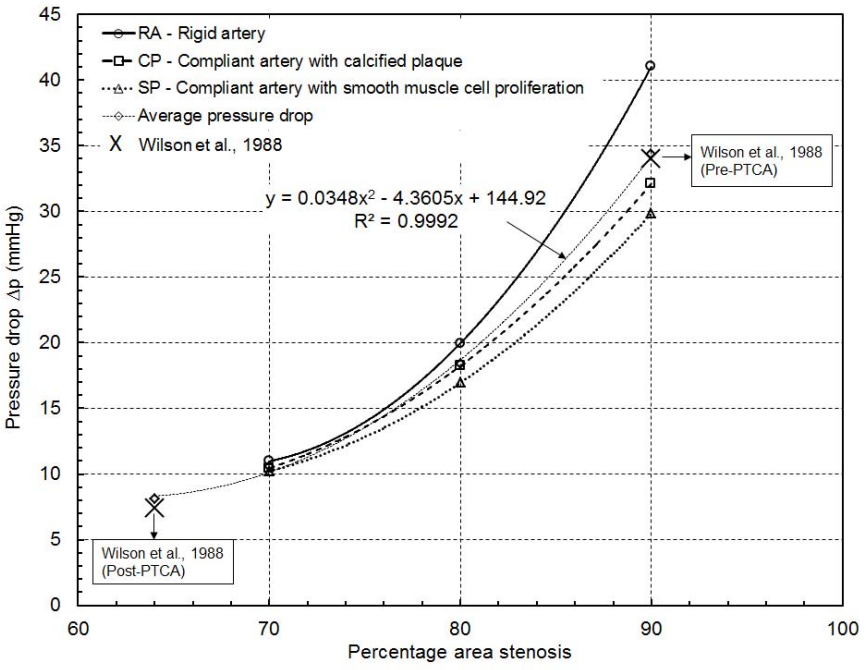

Figure 7: Effect of compliance on the overall pressure drop at different stenosis severities

the rigid artery, the Δp elevated from 11.0 to 19.9 mmHg, an 81% increase, as the stenosis severity increased from 70% area stenosis to 80% area stenosis. The Δp further increased by 2.1 times, from 19.9 mmHg for 80% area stenosis to 41.0 for 90% area stenosis. For CP, the Δp increased from 10.4 mmHg for 70% area stenosis to 18.2 mmHg, a 75% increase, for 80% area stenosis. Similarly, the value of Δp elevated by 76%, from 18.2 mmHg for 80% area stenosis case to 32.1 mmHg for the 90% area stenosis case. For SP, as the stenosis severity increased from 70% area stenosis to 80% area stenosis, the Δp increased from 10.2 mmHg to 16.9 mmHg, a 66% increase. The Δp further increased by 76% from 16.9 mmHg to 29.8 mmHg as the severity of stenosis increased from 80% area stenosis to the 90% area stenosis.

The average Δp values for RA, CP, and SP were calculated. The average Δp values for 70%, 80%, and 90% area stenosis were determined to be 10.5 mmHg, 18.4 mmHg, and 34.3 mmHg, respectively. Since the difference in Δp for 70% area stenosis between the RA (maximum Δp case; 11.0 mmHg) and SP (minimum Δp case; 10.2 mmHg) models was considerably small (∼7%), we assumed that the computed Δp for 64% area stenosis for the RA model (8.12 mmHg) to be nearly

the same for other wall-stenosis models. A quadratic curve was fitted ($R^2 = 0.999$) to the average Δp values to obtain the variation of Δp with stenosis severity (Fig. 7).

It may be noted that RA and SP represent the physiologic limiting cases of arterial wall stiffness that can be found in human population. Here RA represents an artery with arteriosclerotic (near rigid) plaque as observed in the older patients (35). In contrast, SP represents a less rigid (or more compliant) plaque that can happen due to smooth muscle cell proliferation. It was considered appropriate to compare our results of averaged Δp with the *in vivo* Δp values before and after angioplasty as reported by Wilson et al. (30). The measured *in vivo* Δp value for pre-angioplasty (90% area stenosis) was 34 mmHg whereas for post-angioplasty (64% area stenosis) was 7.4mmHg. The average Δp obtained from the curve (Fig. 7) for 90% area stenosis was 34.2 mmHg and 64% area stenosis was 8.3 mmHg. These calculated Δp values were within 1% for pre-angioplasty case and within 11% for post-angioplasty case.

Pressure Drop-Stenosis Relationship under Hyperemic Flows. It could be observed from Fig. 7 that the rigid stenosed artery caused a higher Δp than the compliant cases. All compliance cases were compared with the baseline rigid artery (RA) case. At 70% area stenosis, for a mean hyperemic flow rate (Q) of 175 ml/min (30), the Δp decreased by 5.7% for CP and by 7.8% for SP. For 80% area stenosis, a decrease in Δp value of 9.3% for CP and 17.7% for SP were observed at a mean hyperemic Q of 165 ml/min (30). A wider variation in the Δp was observed for 90% area stenosis. For a mean hyperemic Q of 115 ml/min (30), the Δp decreased by 27.7% for CP and 37.6% for SP in case of 90% area stenosis. The compliance of the throat in the compliant cases (Fig. 5) accounts for the lesser Δp for all the three coronary stenosis severities. The compliant artery with smooth muscle cell proliferation (SP) showed a lesser Δp as compared to the compliant artery with calcified plaque (CP) for all stenosis severities. When comparing SP in relation to CP, the Δp was lesser by 2.0%, 7.7% and 7.7% at 70%, 80% and 90% area stenoses, respectively. This was due to the higher compliance (Fig. 5) observed for SP.

4 Discussion

The Δp across a stenosis is measured during angioplasty procedures as a hemodynamic endpoint in determining the severity of the lesion and the effectiveness of the intervention. The Δp calculated across coronary stenoses were comparable with the previous studies (15, 17). However, these studies did not consider the effect of arterial wall-stenosis compliance on the hemodynamic parameters under hyperemic flow conditions. Hence, the present study improves on the previously reported data by quantifying the influence of arterial wall-stenosis compliance on the pressure

drop under hyperemic flows across coronary artery stenoses. A significant variation in the Δp was observed with various compliant models. These variations were due to the compliant nature of the throat section that resulted in a lesser Δp for the compliant models. While the Δp decreased with increase of compliance in the plaque region, its value elevated with increase in stenosis severity as reported in several previous studies.

The plaque irregularities such as wall roughness, lumen dissections and intimal flaps were not considered in this study. The lesion curvatures and vessel bending due to heart motion were also not accounted for in this study. The guidewire obstruction effect studied by Back et al. (3), Banerjee et al. (13, 22) and Roy et al. (17) have shown that presence of guidewires and catheters also influence the pressure and flow measurements. The effects of the above mentioned factors along with compliance need to be considered during future studies. The significant variation in Δp, particularly for higher stenosis cases, at hyperemic flow influences the functional diagnostic parameters, which are often used to assess the severity of a coronary artery stenosis. In the future, the effect of compliance on the diagnostic parameters will be evaluated.

5 Conclusion

The purpose of this study was to evaluate the variation in the Δp for hyperemic flow across various compliant stenosed coronary artery models. A decrease in Δp by 5.7%, 9.3%, and 27.7% at 70%, 80%, and 90% area stenoses, respectively was observed for the compliant artery with calcified plaque when compared with the rigid artery model. A similar trend was observed for the compliant artery with smooth muscle cell proliferation with a larger decrease in Δp of 7.8%, 17.7%, and 37.6% at 70%, 80%, and 90% area stenoses, respectively when compared with the rigid artery model. Higher compliance at the throat of the stenosed artery resulted in the reduction of Δp across the stenosis. Hence, the Δp decreased with increase in compliance. Accordingly, a reduction in the range of 2% - 7% was observed for the smooth muscle cell proliferation case when compared with the calcified plaque case. These variations in Δp could affect the diagnostic parameters which are often used to determine the functional severity of a lesion. Large variations in diagnostic parameters caused by the arterial wall-stenosis compliance from intermediate to severe stenosis severity may result in misinterpretation and misdiagnosis of the coronary artery flow impairment.

References

1. Lloyd-Jones D, Adams RJ, Brown TM, Carnethon M, Dai S, De Simone G, Ferguson TB, Ford E, Furie K, Gillespie C*, et al.* (2009) *Circulation*.
2. Kern MJ, Lerman A, Bech JW, De Bruyne B, Eeckhout E, Fearon WF, Higano ST, Lim MJ, Meuwissen M, Piek JJ*, et al.* (2006) *Circulation* 114, 1321-1341.
3. Back LH, Kwack EY, & Back MR (1996) *J Biomech Eng* 118, 83-89.
4. Young DF & Tsai FY (1973) *J Biomech* 6, 395-410.
5. Mates RE, Gupta RL, Bell AC, & Klocke FJ (1978) *Circ Res* 42, 152-162.
6. Cho YI, Back LH, Crawford DW, & Cuffel RF (1983) *J Biomech* 16, 933-946.
7. Deshpande MD, Giddens DP, & Mabon RF (1976) *J Biomech* 9, 165-174.
8. Siegel JM, Markou CP, Ku DN, & Hanson SR (1994) *J Biomech Eng* 116, 446-451.
9. Back LD, Radbill JR, & Crawford DW (1977) *J Biomech* 10, 339-353.
10. Steinman DA (2004) *Curr Drug Targets Cardiovasc Haematol Disord* 4, 183-197.
11. Banerjee RK, Cho YI, & Back LH (1993) *J Biomech Eng* 115, 316-326.
12. Banerjee RK, Gonzalez CF, Cho YI, & Picard L (1996) *Acad Radiol* 3, 202-211.
13. Banerjee RK, Back LH, Back MR, & Cho YI (1999) *J Biomech Eng* 121, 281-289.
14. Banerjee RK, Back LH, Back MR, & Cho YI (2000) *J Biomech Eng* 122, 310-320.
15. Banerjee RK, Back LH, & Back MR (2003) *Biorheology* 40, 613-635.
16. Banerjee RK, Back LH, Back MR, & Cho YI (2003) *Biorheology* 40, 451-476.
17. Roy AS, Banerjee RK, Back LH, Back MR, Khoury S, & Millard RW (2005) *Am J Physiol Heart Circ Physiol* 289, H392-397.

18. Sinha Roy A, Back LH, & Banerjee RK (2006) *J Biomech* 39, 853-864.

19. Ashtekar KD, Back LH, Khoury SF, & Banerjee RK (2007) *J. Med. Devices* 1, 185-207.

20. Banerjee RK, Sinha Roy A, Back LH, Back MR, Khoury SF, & Millard RW (2007) *J Biomech* 40, 652-662.

21. Sinha Roy A, Back MR, Khoury SF, Schneeberger EW, Back LH, Velury VV, Millard RW, & Banerjee RK (2008) *J Surg Res* 150, 24-33.

22. Banerjee RK, Ashtekar KD, Helmy TA, Effat MA, Back LH, & Khoury SF (2008) *Biomed Eng Online* 7, 24.

23. Banerjee RK, Ashtekar KD, Effat MA, Helmy TA, Kim E, Schneeberger EW, Sinha RA, Gottliebson WM, & Back LH (2009) *J Invasive Cardiol* 21, 511-517.

24. Peelukhana SV, Back LH, & Banerjee RK (2009) *J Biomech*.

25. Bathe M & Kamm RD (1999) *J Biomech Eng* 121, 361-369.

26. Tang D, Yang C, Kobayashi S, Zheng J, Woodard PK, Teng Z, Billiar K, Bach R, & Ku DN (2009) *J Biomech Eng* 131, 061010.

27. Bluestein D, Alemu Y, Avrahami I, Gharib M, Dumont K, Ricotta JJ, & Einav S (2008) *J Biomech* 41, 1111-1118.

28. Valencia A & Villanueva M (2006) *International Communications in Heat and Mass Transfer* 33, 966-975.

29. Valencia A & Baeza F (2009) *International Communications in Heat and Mass Transfer* 36, 137-142.

30. Wilson RF, Johnson MR, Marcus ML, Aylward PE, Skorton DJ, Collins S, & White CW (1988) *Circulation* 77, 873-885.

31. Back LH & Denton TA (1992) in *Adv Bioeng* (ASME BED), pp. 337 - 340.

32. Cho YI & Kensey KR (1991) *Biorheology* 28, 241-262.

33. Gradus-Pizlo I, Bigelow B, Mahomed Y, Sawada SG, Rieger K, & Feigenbaum H (2003) *Am J Cardiol* 91, 27-32.

34. Bathe KJ (2007) *Theory and Modeling Guide, Vol I and II: ADINA and ADINA-F* (ADINA R & D, Inc., Watertown, MA).

35. Alfonso F, Macaya C, Goicolea J, Hernandez R., Segovia J, Zamorano J, Banuelos C, & Zarco P (1994) *J Am Coll Cardiol* 23, 879-884.